scientific reports

Check for updates

OPEN

Cardaria draba subspecies *Shalepensis* exerts in vitro and in silico inhibition of α-glucosidase, TRP1, and DLD-1 proliferation

Ahmet Buğra Ortaakarsu[1]✉, Özlem Bakır Boğa[2] & Esabi Başaran Kurbanoğlu[2]

In this study, in vitro enzyme activity assays were performed to investigate the inhibitory effects on α-glucosidase and tyrosinase-related protein 1, while in silico molecular docking, molecular dynamics, and protein dynamics analyses were performed to provide information on molecular mechanisms. According to information obtained from in silico approaches, inhibition properties are responsible for conformational changes in protein structures, occupation of the active site cleft by the dominant compounds in the extract, as well as long-term changes in protein folding due to departure from the usual motion. The IC_{50} values of *Cardaria draba* (L.) DESV. subsp. *Chalepensis* (L.) extract for α-glucosidase and tyrosinase-related protein 1 were determined to 1.89 ± 0.13 µg/ml and 1.53 ± 0.13 µg/ml, respectively. In addition, the IC_{50} value of the antiproliferative effects of the extract on DLD-1 colon cancer cells was found to be 6.9 µg/mL. Preclinical trials are warranted to validate the extract's therapeutic potential. These findings suggest that *Cardaria draba* extract exhibits enzyme inhibitory and antiproliferative properties, warranting further investigation for its potential role in therapeutic interventions. Further research, particularly in vivo studies, is required to explore the potential of this extract to address DLD-1.

Keywords *Cardaria draba* L., Enzyme inhibition, Colon cancer, Molecular dynamics, Molecular docking

Complex metabolic dysregulation, characterised by uncontrolled insulin resistance, impaired sugar production by the liver and disturbances in the balance of production of hormone-like compounds such as leptin and adiponectin secreted by fat cells, leads to systemic hyperglycaemia, wear and tear of the walls of blood vessels and the gradual failure of the insulin-producing β-cells of the pancreas due to overload[1]. Concurrently, aberrant melanogenesis, orchestrated through dysregulated tyrosinase-related protein 1(TRP1) and tyrosinase-related protein 2(TRP2) catalysis and hostile microenvironments, fosters pathological hyperpigmentation and formation of skin lesions[2–4]. Such intricate pathophysiological milieus transcend simplistic etiologies, integrating molecular cascades of chronic inflammation, advanced glycation end-product deposition, and altered intracellular signaling[5]. Conventional pharmacotherapeutics often exhibit suboptimal specificity, bioavailability, and tolerability, underscoring an urgent impetus to identify alternative modalities capable of concurrently modulating these enzymatic targets[6]. This necessitates innovative, evidence-driven strategies to refine pharmacotherapeutic interventions targeting multifactorial metabolic dermatoses.

In the pursuit of novel inhibitors, a wide range of natural products have garnered attention due to their structural diversity, bioavailability, and reduced adverse effects compared to synthetic agents[7]. Among the numerous botanical species, *Cardaria draba* (L.) DESV. subsp. *Chalepensis* (L.) is a notable member of the Brassicaceae family, distinguished by its rich phytochemical composition, including flavonoids and phenolic compounds with potent biological activities[8]. *Cardaria draba* (L.) DESV. and its subspecies *C. draba* (L.) DESV. subsp. *chalepensis* (L.) are morphologically, ecologically and genetically very similar, but differ in some aspects such as fruit shape (heart-shaped vs. lenticular), distribution range and polyploidy level (chromosome number)[9,10]. The subspecies mostly prefers moderately humid habitats, while the parent species has a wider ecological tolerance[10]. Furthermore, although the genetic similarity is high, the subspecies has a higher level of polyploidy. Therefore, both plants are closely related taxa that can only be distinguished by distribution and morphological details[11]. The *C. draba* (L.) DESV. extract was reported in previous studies with phenolic content of 64.32 µgGAE/mg and flavonoid content of 141.47 µgQE/mg[12]. The antioxidant activity, antimicrobial

[1]Department of Chemistry, Faculty of Science, Gazi University, Ankara, Turkey. [2]Department of Biology, Faculty of Science, Ataturk University, Erzurum, Turkey. ✉email: bugra@ortaakarsu.com

properties, acetylcholinesterase, butyrylcholinesterase, α-glucosidase, α-amylase, and tyrosinase enzyme inhibition property of the main species extract were also reported[12,13].

Despite the growing interest in phytochemicals as potential enzyme inhibitors, there has been a paucity of research examining the α-glucosidase and TRP1 inhibitory profiles of *C. draba* extracts and the underlying molecular mechanisms responsible for these activities. In diabetic conditions, insulin imbalances and metabolic stress may affect the regulation of TRP1 in melanin synthesis, contributing to impaired skin pigmentation and thus increased risk of diabetic complications[14–16]. While α-glucosidase inhibition is studied in the literature for the treatment of diabetes, TRP1 inhibition is an important target for hyperpigmentation, which is one of the diseases caused by diabetes[17–19]. *C. draba*, has the potential for dual enzyme inhibition in terms of its phenolic and flavonoid compound content.

The development of cholecystic neoplasms, which is hypothesized to be related to diabetes, is a global problem in terms of both quality of life and survival rates[20]. The efficacy of colon cancer treatment in patients with diabetes constitutes a distinct problem due to the challenges associated with managing both conditions concurrently. The employment of treatment modalities characterized by a minimal adverse effect profile, encompassing phytochemistry and natural extracts, represents a significant potential for utilization in both treatment regimens and as an adjunctive approach[21,22].

The present study aims to provide a comprehensive evaluation of *Cardaria draba* (L.) DESV. subsp. *Chalepensis* (L.) extract as a dual-function inhibitor targeting both α-glucosidase and TRP1, while also exerting selective antiproliferative activity on DLD-1 colon cancer cells. This subspecies of *C. draba* was preferred because it has significant potential for phenolic and flavonoid content, which are reported to be different from the main species and other subspecies. We combine classical in vitro enzyme inhibition assays with advanced computational approaches, including molecular docking, MD simulations, and protein dynamics analyses, to elucidate the binding modes, structural alterations, and conformational constraints induced by the extract's active compounds. By correlating these findings at the molecular level with the observed inhibitory and antiproliferative effects, we aim to position *C. draba* extract as a valuable candidate for the therapeutic and supportive management of metabolic and dermatological disorders, as well as for integrative strategies targeting related malignancies. This multidisciplinary investigation brings together insights from phytochemistry, molecular pharmacology, and computational biology, laying the foundation for future research on the use of plant-derived compounds in the development of novel, safe, and effective therapeutic agents.

Material and method

Cardaria draba (L.) DESV. subsp. *chalepensis* (L.) O.E. SCHULZ (Brassicaceae), also known as hoary cress or white-top (Family: Brassicaceae). *Cardaria draba* (L.) was collected in July 2023 at Ataturk University, Erzurum (Turkey) at approximately 2000 m altitude and at coordinates 39°54′0″N 41°15′0″E.

The plant material was collected from an unprotected 'nature area' at coordinates specified in the method section and is stored indefinitely at the Department of Biology, Atatürk University (Turkey-Erzurum), under appropriate conditions. Özlem BAKIR BOĞA, Research Assistant at Atatürk University, is responsible for the collected material. The plant material is publicly available upon request, up to 20 g per request, until the total quantity reaches 100 g. Afterwards, material is provided only for internal analysis. Additionally, 50 g of plant material is reserved indefinitely for requests related specifically to this manuscript submitted to Scientific Reports.

Sample preparation

The plant's leaves, stems, and flowers were all utilised. A total of 9.9 g of the sample was weighed and then 100 ml of water was added. The mixture was then placed in a water bath at 60 °C for 12 h. Following this, filtration was performed using Whatman 4 filter paper. The solvent was then removed from the filtered solution using a rotary evaporator (48 °C, 70 rpm). The resulting extracts were stored at +4 °C.

Soxhlet method for GC/MS (Gas chromotography/mass spectrometry)

500 mL of methanol was added to 10 g of powdered plant material and then the extraction process was started at 60 °C. The extraction continued for 18 h. The plant extracts obtained by this process were dried at 48 °C using a vacuum evaporator to remove the solvent[23]. The plant material was pulverized to increase the solvent interaction at the molecular level.

Analysis of GC/MS

To analyze the fatty acid composition of *C. draba* oil, GC/MS (Gas Chromatography/Mass Spectrometry) was employed. The GC/MS analysis was conducted using an Agilent 5975 GC-MSD system equipped with an Innowax FSC column (60 mm × 0.25 mm, 0.25 μm film thickness). Helium gas (1.0 ml/min) was used as the carrier gas. The oven temperature was initially set at 60 °C for 10 min, then programmed to increase at a rate of 4 °C/min until reaching 220 °C, and held constant at 220 °C for 10 min. Finally, the temperature was further increased to 240 °C at a rate of 1 °C/min. The injector temperature was maintained at 250 °C, and the separation ratio was set to 20:1. Mass spectra were recorded at 70 eV, with the mass range maintained between m/z 35–450. GC/MS analyzes were performed for all prepared samples. GC/MS analysis was repeated three times for all samples. The mean values of fat and its morphological characteristics obtained from different locations were compared in detail using analysis of variance (ANOVA). The least significant difference (LSD) method was used to compare the mean values obtained at a 5% significance level[24].

Content analysis of *C. draba* extract by LC-MS/MS method

LC-MS/MS analyses of the phenolic compound were conducted using an Agilent 6460 Triple Quadropole model (Agilent Technologies, Wilmington, DE, USA). The column temperature was maintained at 40 °C. The elution gradient was formed from mobile phase A (water, 0.1% formic acid) and mobile phase B (acetonitrile with 0.1% formic acid). The composition of the mobile phase was 98% A (v/v) from 0 to 4.0 min, 98–80% A (v/v) from 4.0 to 7.0 min, and 80–10% A (v/v) from 7.0 to 14.0 min, a 10% A (v/v) solution was used thereafter. From 14.0 to 15.0 min, a 10–98% A (v/v) solution was employed. Finally, from 15.0 to 17.0 min, a 10–98% A (v/v) solution was used. The total run time was 17 min, with a 4-min equilibration period between each run[25].

Total phenolic determination

A total of 100 µl of plant extract was employed for the determination of total phenolic content. For this purpose, 900 µl of the double-distilled water and 5 ml of Folin-Ciocalteu reagent were combined with 100 µl of plant extract. A standard curve was prepared using gallic acid concentrations ranging from 0.10 to 0.50 mg/ml. All data were expressed as milligrams gallic acid equivalents (GAE) per 100 g of dry extract weight (DW)[26].

Total flavonoid determination

A method involving a combination of aluminum chloride and sodium nitrite was used to determine the total amount of flavonoid compounds in *C. draba* extract. The absorbance of a sample of the plant extract was measured at 510 nm and a reagent blank was used as a reference. The results were expressed in milligrams of catechin equivalent (CE) per 100 g of dry weight (DW), using catechin at concentrations from 0.01 to 0.25 mg/mL, by constructing a calibration curve at various regular concentrations[27].

Enzyme and protein Inhibition studies

TRP1 Inhibition

In in vitro experiments in which 5,6-dihydroxyindole−2-carboxylic acid was used as a tyrosinase substrate, the plant extract's inhibition was evaluated using kojic acid as a positive control. The solution was prepared by adding 150 µL of 5,6-dihydroxyindole−2-carboxylic acid substrate to a 50 mM phosphate buffer solution with a pH of 6.8 to which 25 µL of sample solution consisting of a 2:3 DMSO-water mixture was added. Then, 25 µL of TRP1 (50 units) was added to the medium to initiate the reaction and it was monitored over time. Kinetic absorbance measurements were taken at a constant temperature of 25 °C and were performed at 475 nm using a microplate reader. Data were recorded at 30-second intervals and monitored for 10 min. The inhibition effect was determined as "percent inhibition" using the formula below and expressed numerically[28].

$$\% \text{ inhibition } = [(A_{control} - A_{sample}) / A_{control}] \times 100$$

α-glucosidase inhibition activity

The 4-p-nitrophenyl-a-D-glucopyranoside (PNPG) method[29] was employed to ascertain whether glycosidase was inhibited and to what extent. For this purpose, plant extracts were combined with glycosidase and incubated for approximately 10 min at 37.5 °C. The PNPG method was then applied, whereby the components were combined with the PNPG compound and allowed to react. Na_2CO_3 was added to halt the reaction, thereby ensuring that the environment was also basic. The absorbance of the plant extracts against the acarbose standard material was then measured. The PNPG method, which is a spectrophotometric method, involved taking spectrophotometric measurements at a wavelength of 405 nm[30].

Cytotoxicity analyzes

The cell line from Amasya Uniculture Collection (ATCC® CCL-221) was used cytotoxicity studies. A 100 µl culture medium was prepared using DLD-1 cells by adding three replicates per well at a density of 1×10^4 cells per well in a 96-well plate, and then incubated for 24 h[31]. 0.5% DMSO was used. Subsequently, the extract prepared with DMSO was added at 2500, 1250, 625, 312 mg/L, i.e., 100 µL per well. The DMSO solution containing negative control was included in the control group. MTT solution was added to the cells at 100 µL per well and incubated for 24 h to evaluate the effects of the added solutions. At the end of this period, the MTT solution was removed from the medium and the reaction was stopped by adding DMSO. At the end of incubation, absorbance values were measured and recorded at a wavelength of 570 nm in a spectrophotometer. The difference between the average value of the wells with cells and the average value of the wells without cells was used in the formula to calculate the percentage of viability. The dose that kills 50% of the culture (IC_{50}) was calculated from the curve of the graph obtained using the values read.

Computational method

Molecular modeling techniques were employed to elucidate the underlying molecular mechanisms examined in in vitro studies. To this end, the components of the extract were subjected to molecular docking, with the resulting complexes then undergoing molecular dynamics simulations. The dynamics of the protein were analyzed by in-depth examination of data from the molecular dynamics simulations. All computational studies followed preparation processes and procedures recognized in the literature[32–35].

Molecular docking

A molecular docking method was employed to assess the affinity of the extract components to enzyme protein structures and to identify the dominant compound responsible for the inhibition effect[36,37].

Preparation of ligands All flavonoid compounds identified through GC/MS analysis of the extract's constituents were prepared for molecular docking. For this purpose, each compound was downloaded from PubChem in three-dimensional form (compounds lacking three-dimensional representation were downloaded in two dimensions and evaluated in the most stable conformation through geometry optimization). Each compound was subsequently imported into the Maestro[38] interface and prepared for molecular docking using the LigPrep[39] module. The procedure entailed estimating the ionization states of the compounds at physiological pH 7.4 using the Epik[40] embedded software, generating the most stable conformations, considering the tautomerization state, and minimizing the energy of the system using the OPLS4[41] force field.

Selection and preparation of protein structuresc Protein structures were selected from proteins with PDB ID:5M8M[42] for tyrosinase-related protein 1 and PDB ID:7KBR[43] for α-glucosidase, taking into account the organism factor, the availability of high-resolution crystal data and their use in current studies.

Prior to their transfer to the Maestro interface, the two protein structures were surrounded by water molecules in accordance with the protein structures, using HydraProt[44]. It was trained on 4,000 crystal data and 1,743,108 experimental water molecules from the HydraProt Protein Data Bank and used to surround protein structures with water molecules at the correct positions.

The protein structures were transferred to the Maestro interface and the necessary preparations for molecular docking were carried out. A specific procedure was followed for the preparation. The procedure performed using the Protein Preparation Wizard[45] included the estimation of the ionisation states of the proteins at pH 7.4, the addition of missing residues in the best conformations, the formation of disulfide bonds, the preprocessing by addition of hydrogens, the subsequent optimisation of hydrogen bonds to pH 7.4, and the minimisation using the OPLS4 force field.

Flexible docking study All of the compounds in the plant extract were docked to the protein structures of TRP1 and Glucosidase using the Induced Fit Docking (IFD)[46] tool. The IFD tool uses the Glide module and all calculations were performed in the advanced sampling setting, with 80 exposures requested. The docking was conducted at the active sites of the protein structures, which are the locations where the cognate ligands were already present.

Molecular dynamics

The evaluation of protein-ligand complexes obtained by molecular docking was conducted using molecular dynamics simulations, a more advanced research method that enables the study of protein-ligand complex movements within a similar physiological environment over a short time period. This approach allows for the investigation of stability, conformational changes in protein structure, and the impact of the ligand on the inhibition process, among other factors.

System setup The formed protein-ligand complexes were immersed in an orthorhombic solvent box consisting of water molecules of the SPC[47] type with dimensions of 10 Å × 10 Å × 10 Å. Following the addition of sodium and chloride ions to the solvent box to ensure neutralisation, 0.15 M NaCl was added in accordance with the physiological environment[32]. Minimisation was performed in the OPLS4 force field in accordance with molecular dynamics simulations.

Molecular dynamics system protocols Molecular dynamics calculations entail the modelling of a small time step, necessitating a constant number of particles, a constant temperature, and a constant pressure. The constant particle number was achieved by limiting the size of the solvent box, the constant temperature was set to 300 K using a Nose-Hoover[48] thermostat and the constant pressure was set to 1 bar using a Martyna-Tobias-Klein[49] barostat. The molecular dynamics study was performed using the Desmond[50] module and consisted of two phases. These phases were a 2 ps relaxation phase and a 100 ns simulation generation phase. 500 frames (each frame corresponds to 0.2 ns) were requested for α-glucosidase and 2000 frames(each frame corresponds to 0.05 ns) for TRP1. In these MD simulations using the M-SHAKE algorithm, a time step of 2 fs was employed[51]. The request for two different frame values was related to the size of the protein structures and the different preferences ensured the correct use of computational resources, especially for α-glucosidase. Each of the molecular dynamics simulations was repeated four times.

Advanced analysis of protein dynamics

The impact of the primary compounds present in *C. draba* extract on the protein dynamics of both TRP1 and α-glucosidase enzymes was investigated through the analysis of data obtained from molecular dynamics simulations. These simulations employed a range of techniques, including Diffusion Map[52] dimension reduction, Time-Lagged Independent Component Analysis based Free Energy Surfaces (TICA-FES)[53]. The scripts used are available at https://github.com/cannabinoid13/MDScripts.

Molecular mechanics with generalised born and surface area solvation (MM/GBSA)

In the molecular dynamics simulation of protein-ligand complexes, the free energy was calculated using the MM/GBSA method for each frame of the simulation. The energy values obtained were also incorporated into the Diffusion Map graphs. The MM/GBSA calculation was conducted in the VSGB[54] solver model, employing the following equation with the Prime[55] Module.

$$\Delta G = E_{complex}\,(\text{minimized}) - [E_{ligand}\,(\text{minimized}) + E_{receptor}\,(\text{minimized})]$$

Results

Total phenolic content (TPC) and total flavonoid content (TFC) results

This study demonstrated the total phenolic and total flavonoid content in aqueous extracts of *C. draba*. The total phenolic content was quantified as 35.35 ± 0.51 mg GAE/g aqueous extract (mg gallic acid equivalent in g dried extract). The total flavonoid content of the water extracts was determined as 33.58 ± 1.23 mg CE/g (mg quercetin equivalent in g dried extract).

Gas chromatography–mass spectrometry (GC/MS) results

The analysis revealed that the compound allyl isothiocyanate constituted 74.07% by weight of the plant extract. The thiocyanic acid, 2-propenyl ester compounds accounted for 8.45% of the extract's weight, while other components represented less than 2% of the total extract weight. Please refer to the Supporting Information for a comprehensive list of all compounds present in the plant extract.

Liquid chromatography–mass spectrometry (LC/MS) results

The LC/MS results of the saturated extract solution of *C. draba* showed that from the most abundant to the least abundant vitexin (8561.6281 ng/mL), luteolin (569.0751 ng/mL), cyanidin−3-*O*-glucoside (446.8699 ng/mL), and a phenolic compound, rosmarinic acid (1.0837 ng/mL), also entered the ranking. Since we focused only on flavonoids and phenolic compounds, both known to have high biological activity, seven of the compounds are presented in Table 1. Full results are available in Supporting Information.

Enzyme and protein inhibitory activities

The impact of *C. draba* extract on α-glucosidase and TRP1 was assessed through in vitro experimentation. The outcomes of these in vitro experiments were then compared with the results of analogous experiments conducted with the acarbose compound for α-glucosidase. The outcomes of the experiments performed with the kojic acid compound for TRP1 were similarly compared. The data points were fitted to a sigmoid curve, allowing the inhibition rates of the enzymes to be accurately and clearly determined. The fitted curve was generated using a four-parameter logistic (4PL) model. Thus, IC_{50} values, correlation coefficients (R^2) and areas under the curve (AUC) were accurately determined. In addition, a confidence interval was determined for each experiment using the bootstrap method and determine the standard deviation of the IC_{50} values.

The IC_{50} value of the acarbose compound employed as a positive control for α-glucosidase was determined to be 2.74 ± 0.11 µg/ml, exhibiting a coefficient of determination (R^2) of 0.994 and an area under the curve (AUC) of 273.99. The IC_{50} value of *C. draba* extract in in vitro experiments was determined to be 1.89 ± 0.13 µg/ml, with a coefficient of correlation (R^2) of 0.995. Additionally, the area under the graph (AUC) was determined to be 232.31. The IC_{50} value of the positive control compound kojic acid employed in the experiments concerning the TRP1 was determined to be 1.70 ± 0.48 µg/ml, with an R^2 value of 0.988. The AUC value was 214.51. The IC_{50} value of the *C. draba* extract was determined to be 1.53 ± 0.13 µg/ml with an R^2 value of 0.999, and the AUC value was 191.76. Figure 1 provides a comprehensive illustration of the aforementioned data in a clear and concise manner.

One-way ANOVA revealed a significant difference in IC_{50} values among *C. draba* extract, acarbose, and kojic acid ($F(2,6) = 10.64$, $p = 0.01$). Tukey's post-hoc HSD test confirmed that the IC_{50} of acarbose was significantly higher than that of *C. draba* extract and kojic acid ($p < 0.05$ for both comparisons). In contrast, there was no significant difference between the IC_{50} values of *C. draba* extract and kojic acid ($p > 0.05$).

Cytotoxicity results

As a result of the analysis performed using the MTT method, the cytotoxic effect of the plant extract used on the Human Colon Cancer Cell Line (DLD-1) is given in Table 2. Viability was determined to be 22.23% with 312 µg/mL extract and 38.94% with 625 µg/mL extract. The 87.61% viability in the treatment with 1250 µg/mL extract decreased to 80.26% after the treatment with 2500 µg/mL. It was observed that viability increased when the plant extract was applied to DLD-1 cells at concentrations of 1250 and 2500 µg/mL. A decrease in cell viability was observed at 312 and 625 µg/mL. Accordingly, it was determined that the ideal concentration of the extract applied to DLD-1 cells were 312 and 625 µg/mL. The IC_{50} value of the extract is 767 µg/mL for the DLD-1 cell line. Additionally, advanced statistical modeling, including ANOVA with Bonferroni corrections, validated the extract's effect with high significance ($p < 0.001$).

Molecule name	Final cons.(ng/mL extract solution)
Vitexin	8561.6281
Luteolin	569.0751
Cyanidin-3-*O*-glucoside	446.8699
Apigenin	108.6049
Quercetin	60.4772
Isorhamnetin	58.1453
Rosmarinic acid	1.0837

Table 1. Most abundant phenolic compounds in quantitative analysis results.

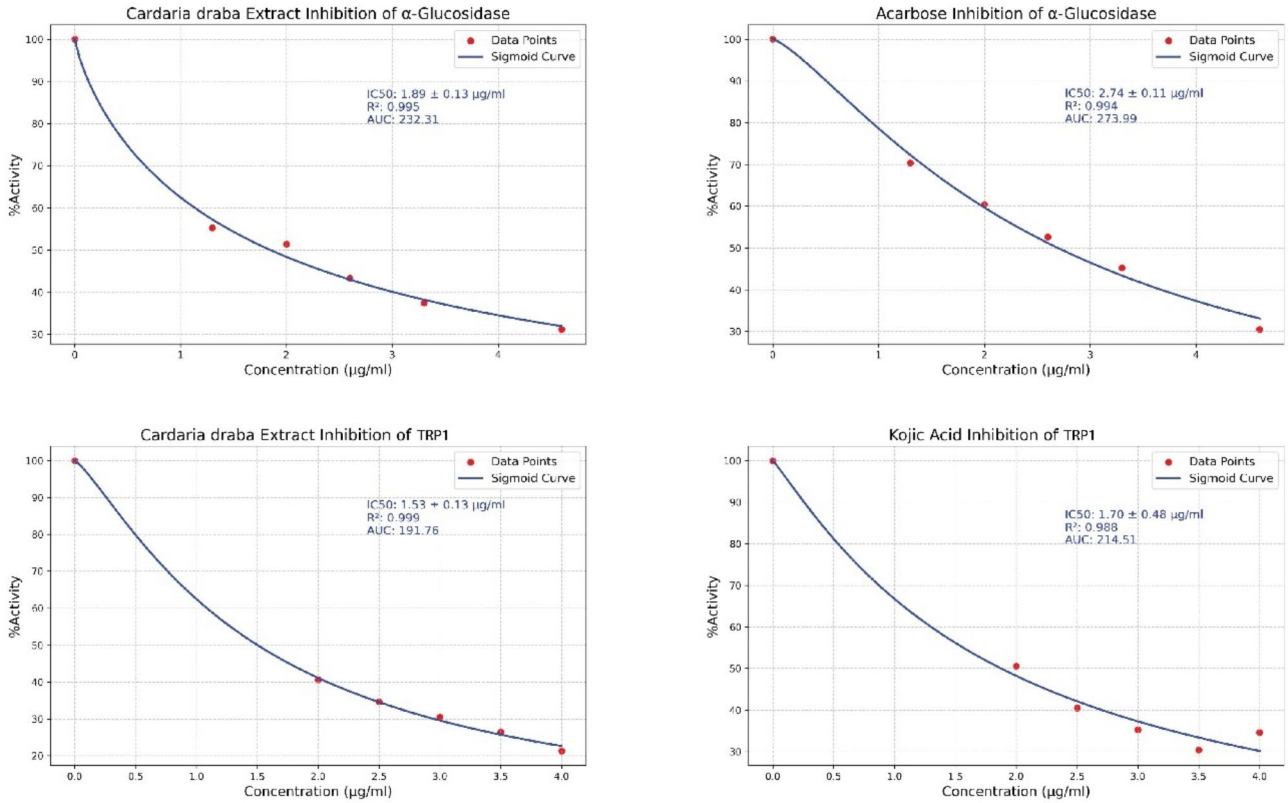

Fig. 1. The inhibition curves of α-glucosidase and TRP1 by *C. draba* extract, acarbose, and kojic acid are presented. The IC_{50} values, R^2 coefficients, and areas under the curve (AUC) are provided, demonstrating the inhibitory efficacy of each compound.

Concentration (µg/mL)	Cell viability (%)	% cytotoxicity
312	22.23 ± 1.75	77.77
625	38.94 ± 3.45	61.06
1250	87.61 ± 4.45	12.39
2500	80.26 ± 5.40	19.74

Table 2. The effect of the plant extract on the cell viability of the human Colon cancer cell line (DLD-1) during the 24-h experiment was observed.

Trend change was detected in the cell viability value at 2500 µg/mL concentration in Table 2. This trend change was evaluated as the change in the effectiveness of the extract on cancer cells as a result of exceeding the threshold concentrations of some compounds in the plant extract related to the defence mechanisms of the cell line.

Molecular docking

For accurate molecular docking of α-glucosidase and TRP1, validation was performed by removing and reinserting the cognate ligand. Flexible docking was performed for both enzymes using the settings shown in Supporting Information - Figure S1. In the results obtained, the same compounds were found to be prominent for both enzymes. These compounds are cyanidin-3-*O*-glucoside, vitexin and rosmarinic acid. All compounds in the extract that can dock to the active sites of TRP-1 and α-glucosidase protein structures, and their docking scores from different poses, are presented in Supporting Information - Table S1.

α-glucosidase docking study

In a molecular docking study to evaluate the affinity of the compounds in the plant extract for the α-glucosidase enzyme, cyanidin-3-*O*-glucoside, vitexin and rosmarinic acid showed that they may have the highest potential affinity. The cyanidin-3-*O*-glucoside compound had higher affinity than the other compounds. Hydrogen bonds (H-bonds) were detected between the α-glucosidase enzyme and the cyanidin-3-*O*-glucoside compound via Asp305, Asp640 and Gln308 residues. The rosmarinic acid compound, in which the pi bond and ester group in the carbon chain structure cause conformational restriction, was found to hydrogen bond with residues

His700, Arg624 and Asp564. Vitexin exhibits a similar conformational arrangement to cyanidin-3-*O*-glucoside. Residues His700, Glu453 and Trp523 form direct hydrogen bonds with Vitexin. Furthermore, Asp702 forms a hydrogen bond through a water bridge. All the aforementioned interactions between the compounds and the protein structure are clearly shown in Fig. 2 together with the functional active protein. Cyanidin-3-*O*-

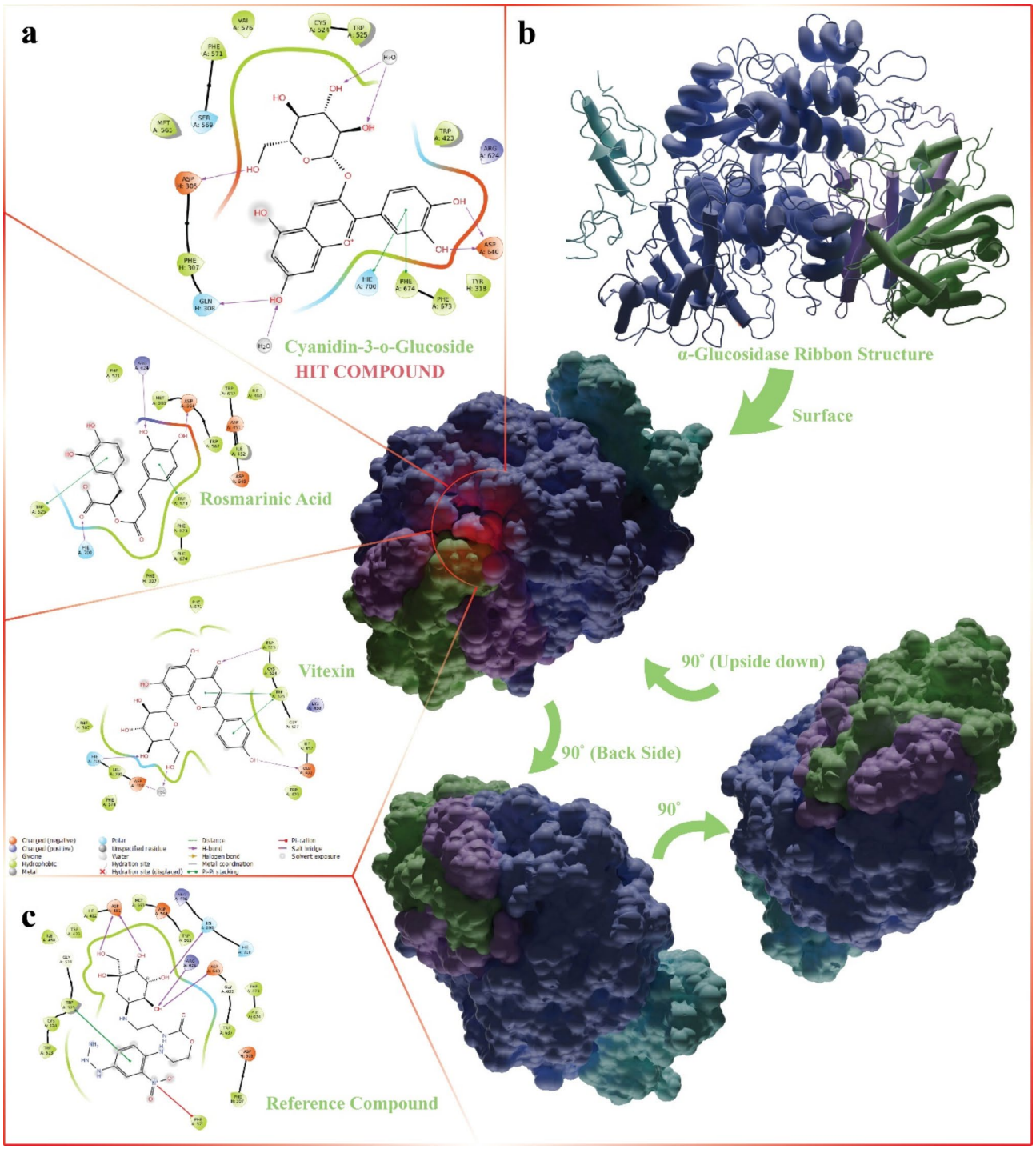

Fig. 2. This section presents the binding modes of the compounds with the highest binding affinity for α-glucosidase, as detected in *C. draba* extract. It also provides details of the α-glucosidase protein structure. (**a**) 2D interaction map (**b**) Ribbon and surface representation of α-glucosidase protein structure. Colours represent different chains. The red spot light shows the exact position of the active site(protein at the centre). Although the protein structure is a dimeric structure, it is shown as a single unit for clarity. (**c**) Binding pose of reference compound with proven efficacy. All of the three-dimensional images in the image were created using the Molecular Nodev4.2.12[56,57] plugin in Blender v4.3.2 (https://www.blender.org/about/website/).

glucoside, rosmarinic acid and vitexin each have the highest docking scores of −10.367 kcal/mol, −9.000 kcal/mol, −8.413 kcal/mol, respectively. The docking score of the reference compound, which proved to be more effective than acarbose, −10.251 kcal/mol.

TRP1 docking study

The molecular docking study for TRP1 shows that there is potential affinity between the compounds in the same order. The most important factor in the inhibition of TRP1 is the coordination between the compounds and Zn^{+2} atoms in the active site. Cyanidin-3-*O*-glucoside compound showed higher affinity than other compounds due to forming H-bonds with residues Gly389, Arg374, Glu216 and Val196. The rosmarinic acid compound formed salt bridges with Arg374 and Arg321 residues and H-bonds with Val196, Arg374 and Ser394 residues. However, its affinity for the TRP1 was found to be relatively low due to its incompatible localization with the protein structure in the active site cleft. It ranked second. Vitexin compound was found to make H-bonds with residues Glu216, Arg374 and Ser394. All interactions between proteins and compounds are shown in Fig. 3. Cyanidin-3-*O*-glucoside, rosmarinic acid and vitexin ligands with the highest docking scores are − 8.492 kcal/mol, − 7.178 kcal/mol, − 5.852 kcal/mol, respectively. The docking score of Kojic Acid used as a reference compound was determined as − 6.743 kcal/mol.

Molecular dynamics

In molecular dynamics studies, the cyanidin-3-*O*-glucoside compound, which showed the highest affinity for both enzymes, was used. All molecular dynamics simulations were followed by trajectory analysis and minimal conformational change was detected for the ligands. In the analysis of molecular dynamics simulations and all further analysis methods, a comparison of protein structures with ligands (Halo Form) and protein structures without ligands (Apo Form) was made.

Root mean square deviation (RMSD) and root mean square fluctuation (RMSF)

RMSD plots are used to align the positions of protein α-carbons across frames of the MD simulation by superimposing their initial positions onto the other frames. Subsequently, the plots for each frame serve as a numerical indicator, of the difference. The analysis of RMSD plots is employed to gain insight into the conformational constraints in protein structure, as well as to elucidate the underlying mechanisms of unusual conformational changes in protein structure. RMSF graphs represent a pivotal analysis method for detecting local fluctuations in protein structures and fluctuations of critical amino acids that affect enzyme dynamics, particularly the active site. Figure 4 presents the RMSD and RMSF data for Apo Forms and Halo Forms for each enzyme.

In the MD simulations, the Halo Form graph of α-glucosidase followed a parallel course with an average RMSD of 2.4 Å, while the Apo Form graph exhibited average RMSD values of 2 Å. The plots showing the RSMD values showed a similar distribution. In the simulations of TRP1, the Apo Form plot showed high RMSD values with very pronounced fluctuations. The Halo Form plot was very stable. In the histogram, Halo Form showed a narrow distribution and Apo Form a wide distribution. This is important evidence that the active site docking of the cyanidin-3-*O*-glucoside compound in its Halo Form causes significant conformational changes in protein dynamics, rendering the enzyme inoperable.

The limited degree of fluctuation observed in the RMSF plots indicates that the cyanidin-3-*O*-glucoside compound is firmly attached to both protein structures. The α-glucosidase enzyme is characterized by a substantial volume and a considerable number of free ends, resulting in frequent and pronounced fluctuations in the RMSF plots. The RMSF plots revealed that the cyanidin-3-*O*-glucoside compound influenced these fluctuations, and significant disparities were observed between the Halo Form and the Apo Form, particularly at residue indexes 600, 750, and 820. The TRP1 exhibited a substantial fluctuation around residue index 50, which was mitigated when in the protein structure in complex with the ligand.

The interactions established in the molecular docking study were found to persist in MD simulations. In these findings, the continuity of hydrogen bonds of Asp305, Ser569 and Trp525 residues in α-glucosidase was determined. While metal coordination was prominent in TRP1, hydrogen bonds were found to be continuous with residues Val196, Gly209, Val211, Asp212, Asn378, Gly389 and Thr391.

Advanced analysis of protein dynamics

The MD simulation data obtained for both enzymes in their Apo Form and Halo Form were subjected to further analyses. These analyses were conducted for a variety of purposes, including the determination of the impact of ligands on protein folding, the investigation of alterations in the energy windows of protein structures, and the examination of differentiation in the coordination of residues that move in a coordinated manner in response to ligand effects.

TICA-FES For the analysis of large conformational changes in protein structures, such as protein folding, TICA-FES analyses with 500 lag values were performed. The graphs shown in Fig. 5 illustrate the long-term large-scale movement of protein structures associated with the cyanine-3-*O*-glucosidine compound in *C. draba* extract.

The α-glucosidase enzyme, with its large and bulky structure, is characterized by many small and important conformational changes in the Apo Form. The Halo Form graph is very different. The irregular structures in the Apo Form are replaced by a deep low energy valley that cuts diagonally across the graph. The TRP1 shows a single deep low energy valley, whereas the Halo Form graph is "split in two", indicating that it is possible to switch between certain basic conformations, but this switching is prevented by a high energy barrier.

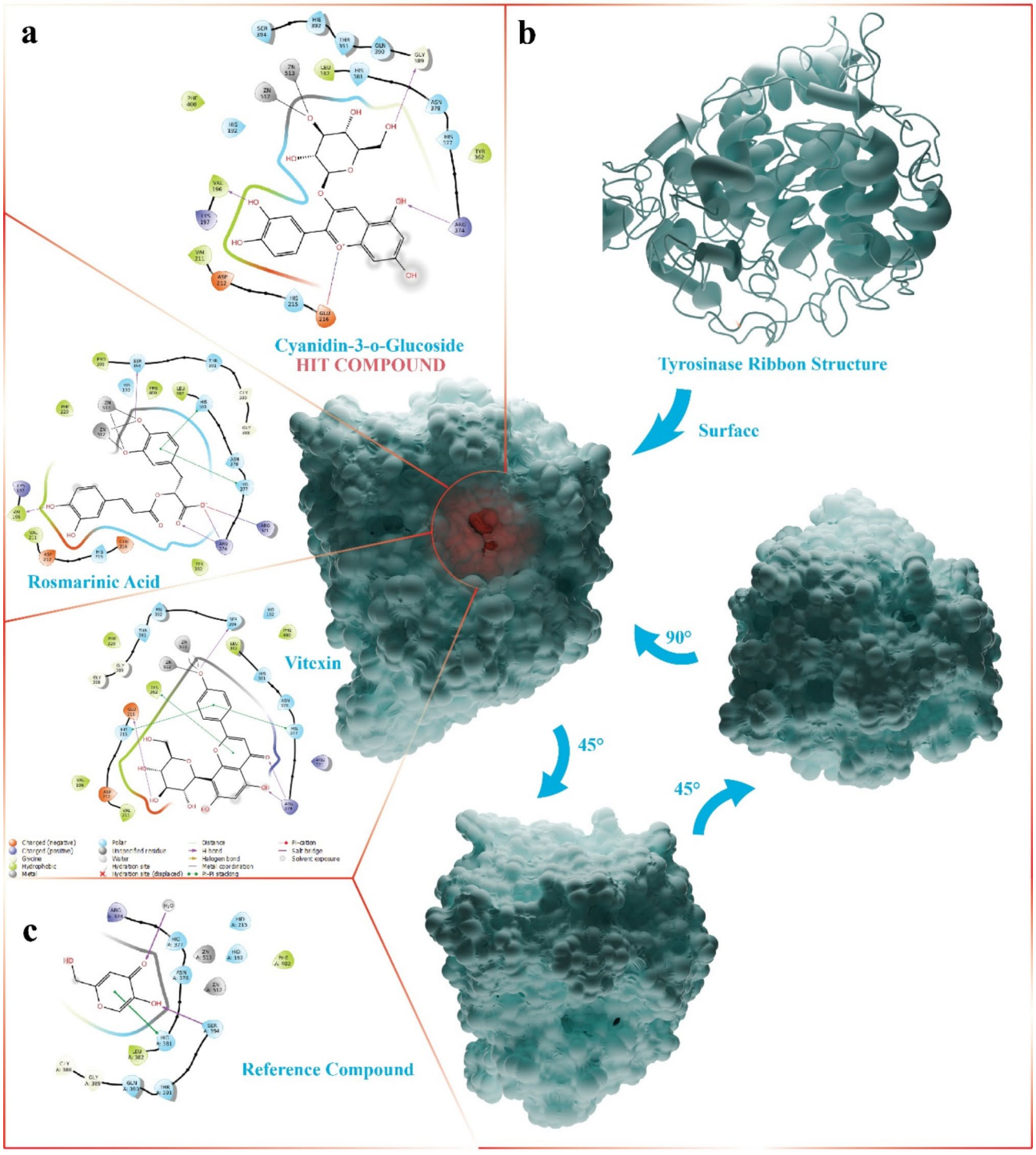

Fig. 3. This section presents the binding modes of the compounds with the highest binding affinity for TRP1, as detected in *C. draba* extract. It also provides details of the α-glucosidase protein structure. (**a**) 2D interaction map (**b**) Ribbon and surface representation of TRP1 structure. The red spot light shows the exact position of the active site(protein at the centre). Although the protein structure is a tetrameric structure, it is shown as a single unit for clarity. (**c**) Binding pose of reference compound with proven efficacy. All of the three-dimensional images in the image were created using the Molecular Node v4.2.12[56,57] plugin in Blender v4.3.2 (https://www.blender.org/about/website/).

Dimensional reduction with MM/GBSA integrated diffusion maps The diffusion map method, a leading dimensional reduction technique, was applied to the free energy values obtained from the MM/GBSA calculation for each frame. Consequently, the most preferred conformations in the diffusion map graphs are clearly identified as the regions where the frames are grouped, and stable conformations are determined by revealing the

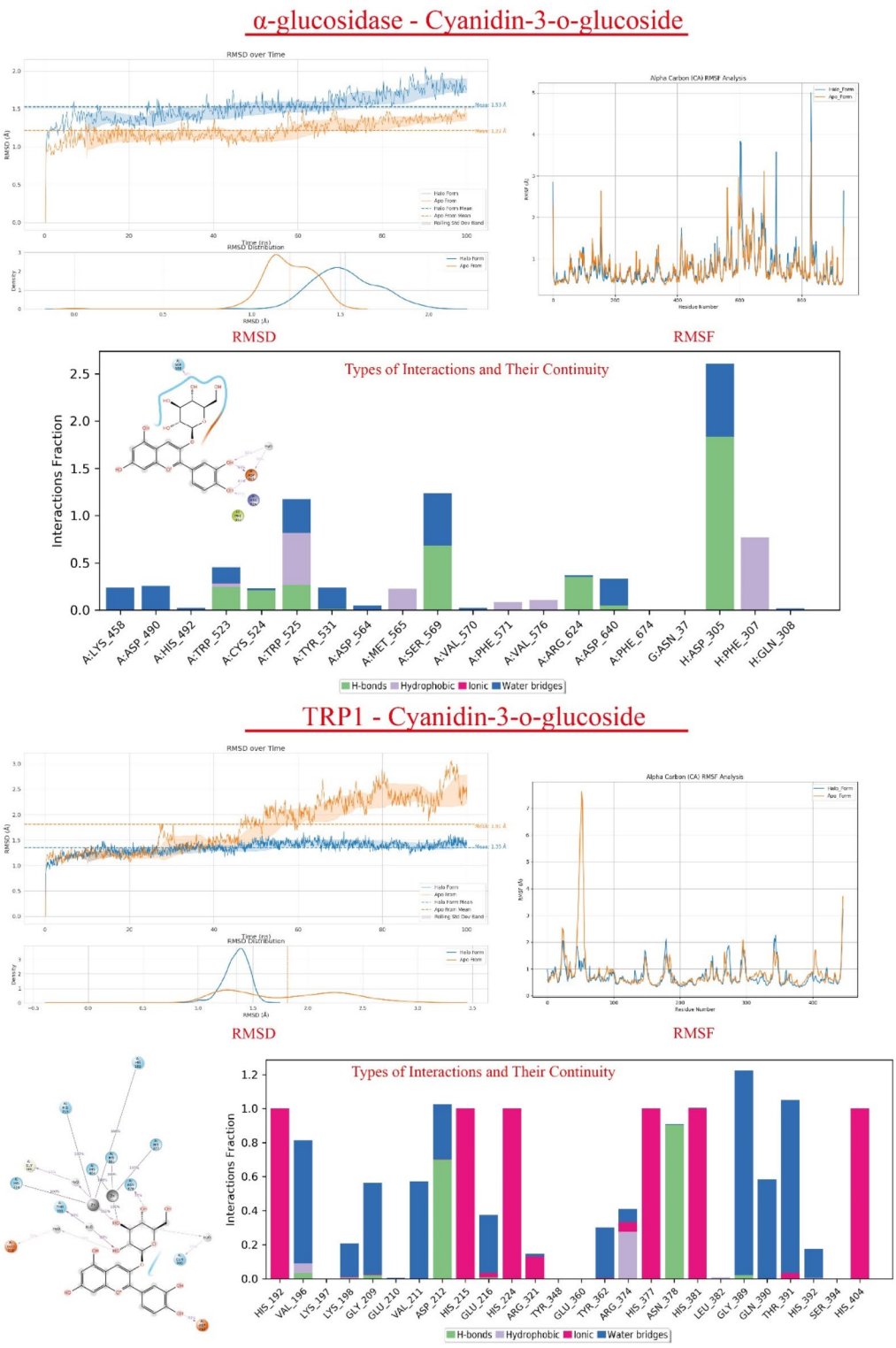

Fig. 4. RMSD, RMSF and interaction plots of MD simulations of cyanidin-3-*O*-glucoside compound docked to α-glucosidase and TRP1.

connection between these groupings and free energy values. As illustrated in Fig. 6, both the MM/GBSA data and the integrated diffusion map graphs are presented.

The α-glucosidase enzyme displays two distinct conformations, characterized by low-energy frames. These two conformations were identified as low energy regions at the initial (5–25 ns) and final (80–100 ns) stages of the MD simulations, with a free energy of -60 kcal/mol as determined by the MM/GBSA approach. In comparison to these low energy regions, frames containing higher energy regions manifested as diffuse conformations. These

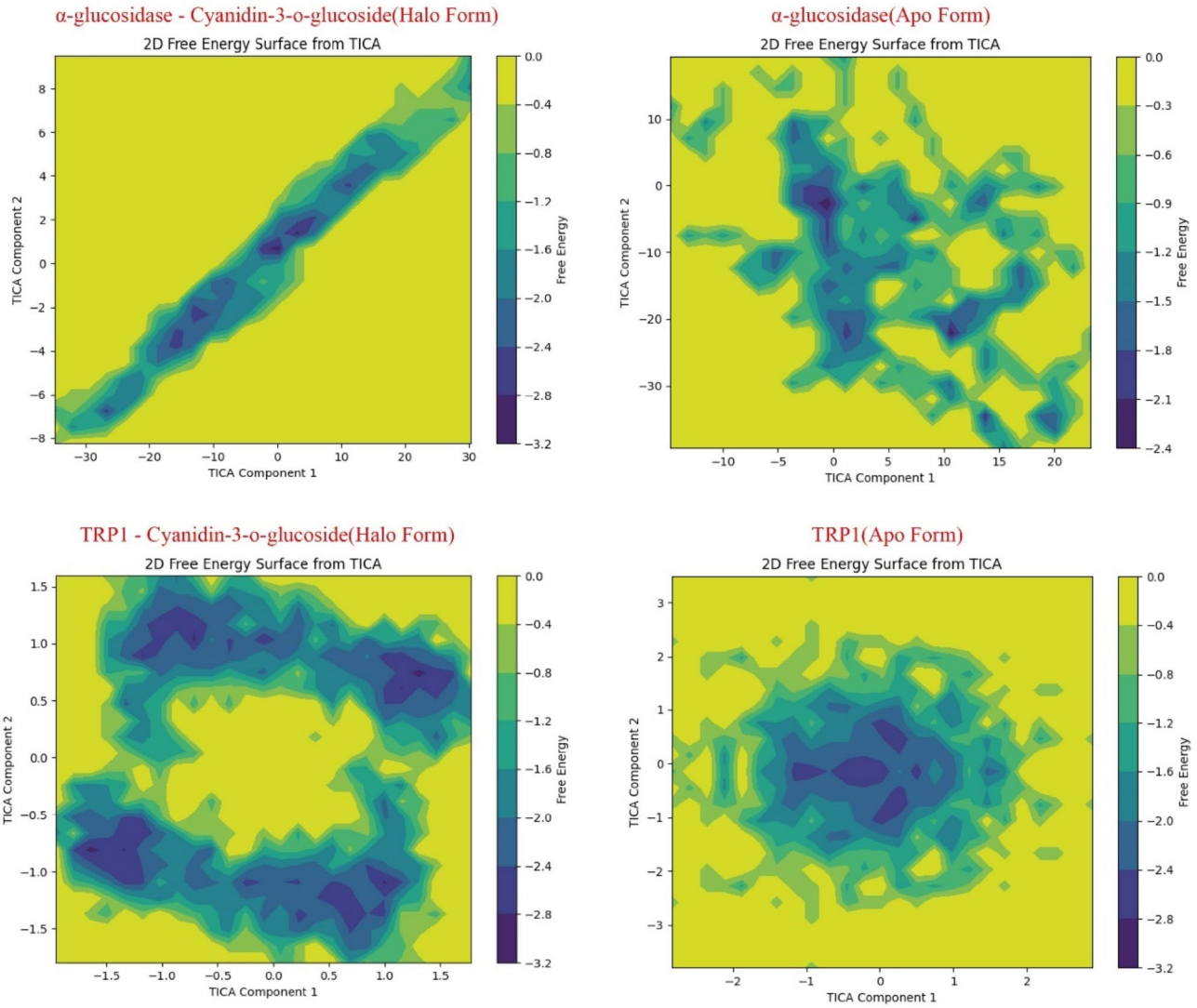

Fig. 5. The impact of the cyanidin-3-*O*-glucoside compound on the α-glucosidase (top) and TRP1 (bottom) enzymes, is illustrated by differentiating between a differentiation between the Apo Form and Halo Form with a prolonged lag TICA-FES. Yellow areas indicate high-energy regions, while dark blue areas indicate low-energy regions.

frames were not preferred in the upper part of the diffusion map and could be characterized as "noise." In the TRP1, a specific region was identified where low energy frames were concentrated. The free energy values of the frames in this area exhibit a high concentration around − 30 kcal/mol, which is the lowest energy value determined for this enzyme in the MM/GBSA calculation. The regions of the graph where conformational similarities differ from each other are distributed as frames with high energy, and showing a diffuse distribution, although their numbers are very few.

The two conformational forms that were identified as preferential for α-glucosidase suggest the long-term dynamics of transitions between them. In contrast, other non-preferred conformations are interpreted as limited dynamic process. For TRP1, the identification of a preferred low-energy structure within the conformational space is significant, as it suggests that the enzyme undergoes dynamic movements that diverge from its typical functionality.

Data on in silico approaches are available as raw data at https://doi.org/10.5281/zenodo.14726884.

Discussion

The analyses of obtained for the aqueous extract of *Cardaria draba* (L.) DESV. subsp. *Chalepensis* (L.) revealed its composition. The compound composition shows the importance of *C. draba* with its high amount of flavonoid compounds and known medicinal uses and its wide range of perspectives on potential targets. This was supported by the measurement of total phenolic compound content as 35.35 ± 0.51 mg GAE/g aqueous and total flavonoid compound content as 33.58 ± 1.23 mg CE/g. In previous studies, it was observed that total phenolic content in different varieties of cabbage belonging to the Brassicaceae family varied between 3.1 and 18.48 mg/g in green

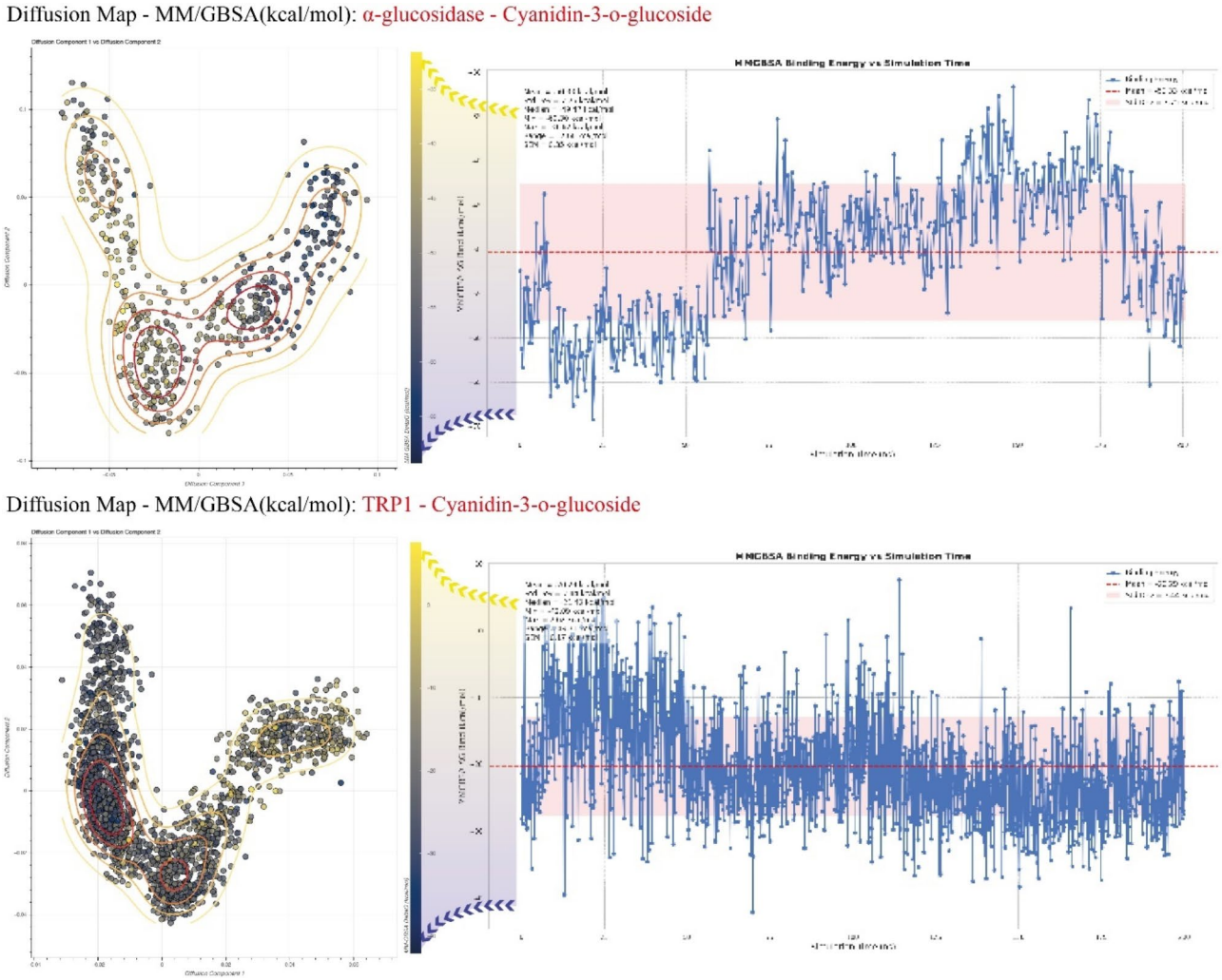

Fig. 6. MM/GBSA data for each frame of the MD simulation of α-glucosidase and TRP1 with cyanidin-3-*O*-glucoside compound and the diffusion map plots connected to these data.

globular varieties, 4.34–17.28 mg/g in green flat varieties, 3.48–15.85 mg/g in purple globular varieties and 8.85–13.3 mg/g in green cylindrical varieties[58]. Another study showed that sprouts such as broccoli and radish exhibited flavonoid content ranging from 25.16 to 25.36 mg CE/100 g, FW[59]. The total phenolic content of *B. oleraceae* L., which belongs to the same family, was shown to be 39.6 ± 0.5 mg GAE/g[60]. In a previous study, the phenolic content of *Sinapis pubescens* L. subsp. *pubescens* was investigated. In the study, it was shown that the leaf (64.06 ± 1.63 mg GAE/g extract) and root (31.02 ± 1.45 mg GAE/g extract) extracts had phenolic content (64.06 ± 1.63 mg GAE/g extract)[61]. Variable plant species have variable secondary metabolite concentrations, which causes variations in how secondary metabolites accumulate in various organs in medicinal plants. The plant's phenolic content varies according on the solvents and techniques used[62].

The results obtained in this study provide striking evidence for the potential of *C. draba* extract to inhibit α-glucosidase and TRP1. In particular, when compared with acarbose, which was used as a positive control for α-glucosidase inhibition, and kojic acid, which was used for TRP1 inhibition, *C. draba* extract was found to have significantly lower IC_{50} values. While the IC_{50} value of acarbose was 2.74 ± 0.11 µg/ml, it was 1.89 ± 0.13 µg/ml for *C. draba*, indicating that the extract exhibited higher inhibition activity. *Brassica oleracea* var. *capitata* L. from the same family showed IC_{50} values of 3.08 mg/mL for α-amylase and 22.63 mg/mL for α-glucosidase[63]. *Crambe tataria* flower extracts, α-amylase and α-glucosidase enzyme inhibitory effects are 3.70 mg/mL and 4.89 mg/mL, respectively[64]. In their study with *Cakile maritima*, which belongs to the Brassicaceae family, they observed an inhibition of α-glucosidase at a rate of 0.16 ± 0.01 mmol ACAE/g extract only in aqueous extracts of the aboveground parts of the plant[65].

Similarly, *C. draba* extract (IC_{50}: 1.53 ± 0.13 µg/ml) showed a stronger inhibition profile compared to kojic acid (IC_{50}: 1.70 ± 0.48 µg/ml) in TRP1. This difference is thought to be due to changes in the active site or surface conformation of the enzymes caused by flavonoids and phenolic compounds present in the extract. *Sambucus ebulus* L. extract showed the highest tyrosinase inhibition (IC_{50} 0.08 mg/mL)[66]. *Brassica oleracea* var. *capitata* f. *rubra* leaf extract showed tyrosinase inhibition with IC_{50}: 1.71 mg/ml[67]. It has been determined that the

chemical contents and partially biological activities of the samples of the same species collected from different localities are different both within themselves and from the studies in the literature. This situation has led to the conclusion that the chemical content of the species, in particular, is greatly affected by the climate conditions and soil structure in which it grows.

The high correlation coefficients obtained (R^2 values of 0.988 and above) show that the four-parameter logistic (4PL) model is highly compatible with the data. The four-parameter logistic model and AUC analyses confirm the statistical validity of the concentration-response relationship, as demonstrated by the relatively high inhibitory potency of *C. draba* extract over a wide dose range in both α-glucosidase (AUC = 232.31 vs. 273.99 for acarbose) and TRP1 (AUC = 191.76 vs. 214.51 for kojic acid). Furthermore, bootstrap analysis enhances the reliability of these IC_{50} and AUC values by providing robust standard errors and confidence intervals, thereby accommodating the high intrinsic variation typical of biological data.

The inhibitory effect of the main species extract of *C. draba* on α-glucosidase is known to be remarkable for the treatment of diabetes and metabolic syndrome. Similarly, inhibition of TRP1 is a strategy used in hyperpigmentation and related dermatological problems (e.g. melasma, age spots, etc.)[68]. Kojic acid is one of the enzyme inhibitors commonly used for this purpose. Therefore, the results obtained in this study show the potential value of *C. draba* extract as an adjuvant or alternative raw material for treatment, especially as it significantly suppresses enzyme activity. Although the effect of *C. draba* on these two enzymes has been partially demonstrated by previous studies, there are still many critical questions about the mechanism of action waiting to be clarified. While the computational part of our study demonstrates the effect of *C. draba* aqueous extract on these two enzymes in a way quite parallel to the known, it has a unique value in terms of the content and effect potential of the crop collected from the region.

However, as frequently emphasised in the literature, the results of in vitro enzyme activities and cell-based experiments should undergo extensive validation processes before being directly transferred to clinical applications. For example, pH changes in the gastrointestinal tract, expression levels of enzymes in different tissues and bioavailability of metabolites can greatly alter the results under in vivo conditions. In addition, the safety profile, interactions and pharmacokinetic properties of long-term use will need to be investigated in detail. Studies in preclinical animal models and phase clinical trials will help to clarify the true therapeutic or supportive role of *C. draba* extract. Potential bioavailability and pharmacokinetic studies together with in vivo studies may give more precise information about the actual potential use of *C. draba* extract, but our current findings are promising. In the section of the study involving computational approaches, the mechanism of action of the dominant compounds in the compound composition of *C. draba* extract was emphasised.

Asp305 residue in the complex formed by α-glucosidase enzyme and Cyanidin-3-*O*-glucoside compound obtained in molecular docking study showed that it behaves as a critical residue by maintaining its continuity in MD study. The continuity of the hydrogen bond formed showed its continuity with the water molecules acting as a bridge. Cyanidin-3-*O*-glucoside exhibits strong enzyme affinity in *C. draba* extract, notably via double coordination with TRP1 metal atoms. Despite lower levels than vitexin, its concentration parallels luteolin. Its ether group fosters flexibility, reinforcing superior binding. Molecular docking confirms robust inhibitory properties, highlighting cyanidin-3-*O*-glucoside's pivotal role in α-glucosidase and TRP1 inhibition. In the complex formed with the TRP1 structure, the interactions were largely with metal atoms and the compound is fixed to the active site area. Cyanidin-3-*O*-glucoside interactions are supported by hydrogen bonding interactions with residues Asp212 and Asn378. It was determined from the MD study that these interactions are continuous.

In the present study, the impact of cyanidin-3-*O*-glucoside compound on large-scale movements, such as protein folding in both enzymes, over an extended period was determined by TICA-FES analysis. The free energy surfaces, determined from time-delayed component analyses, exhibited substantial disparities between the Apo Forms and Halo Forms, serving as pivotal indicators of this distinction. Diffusion maps, which yield more realistic results by integrating free energy values in addition to the probability density-dependent method, indicate conformational confinement by providing the exclusion of other conformations with the frequency of transition between two basic conformational structures for α-glucosidase. Diffusion maps for TRP1 provide information on the preference for low-energy sites in a single basic conformation, indicating the preference of protein dynamics outside its usual motion. This phenomenon was interpreted as the enzyme's inability to function due to the out-of-order movement of protein dynamics on the TRP1 side. The data obtained concerning protein dynamics were corroborated by the analysis of RMSD and RMSF graphs. The α-glucosidase enzyme exhibited a consistent direction in its RMSD graph, while the TRP1 demonstrated a substantial deviation from the standard protein structure motion, exhibiting an increasing trend.

Together with all this information, the experimental data we have obtained in terms of the effect of *C. draba* extract on colourectal adenocarcinoma cancer type, which is interpreted as a serious and significant increase in the incidence with diabetes, is also promising. The antiproliferative effect of the extract on DLD-1 cell line supports the agenda of more comprehensive oncological evaluations.

C. draba extract obtained from above ground has antiproliferative activity in DLD-1 colorectal adenocarcinoma cancer cell line. IC_{50} values of *Brassica juncea*, *Silybum marianum* and *Phaseolus vulgaris* plants, which are also from the Brassicaceae family, showed activity in the range of 0.2–5.5 μg/mL[69]. Compared to control, it slowed down the proliferation rate of cells depending on the dose.In previous studies, cytotoxic effect of root, stem and leaf extracts of *(A) floribundum* from Brassicaceae family was determined as 192.1–157.4 μg/mL, 29.12–26.93 μg/mL and 226.4–80.23 μg/mL at various concentrations after 24 and 48 h on DU-145 prostate cancer cell line, respectively[62]. The IC_{50} values of Garden Cress from the same family against MCF-7, HeLa and MCF-A10 were found to be 12.43 ± 0.95 μg/ml, 13.39 ± 1.01 μg/ml and 42.33 ± 0.97 μg/ml, respectively, highlighting important aspects of its potential anticancer effects[70]. In another study, they showed that the cytotoxic activity of *(B) juncea* was higher than the chemotherapeutic drug doxorubicin on HepG-2, HCT-116, HEP2 and HeLa (IC_{50} = 10.95 ± 1.1 μg, 13.72 ± 1.2 μg, 19.63 ± 1.5 μg, and 12.53 ± 1.1 μg, respectively). Brassica

family components play an important role in cancer prevention due to their activities and properties such as the ability to modify biotransformation enzyme expression[71]. Since the plant extracts are not pure compounds, they showed low cytotoxic effects because of the secondary metabolites they contain. Studies conducted with plants rich in phenolic compounds such as kaempferol, quercetin, 5-hydroxy pyrogallol, apigenin, catechin derivatives, gallic acid, rosmarinic acid, p-coumaric acid, ferulic acid, and ellagic acid suggest that these compounds have anticancer properties against various types of cancer[72]. It is thought that all these phenolic compounds contained in the *(C) draba* extract contributes to its cytotoxic activity. More comprehensive studies are required to determine the mechanisms through which the cytotoxic effect of the extract occurs. The extract of the subspecies *C. draba* in our study showed a moderate effect at IC_{50} 767 µg/mL. In addition to this moderate effect, cancer cell viability at high concentrations of 2500 µg/mL was lower than that at 1250 µg/mL. This unexpected effect was interpreted as the effects of some compounds in the compound composition at high concentrations triggered the defence mechanism of the cancer cell. This is an important finding regarding the applicability of dose-dependent cell viability and may be important for determining the dose threshold of in vivo experiments in future studies.

In this study, the aqueous extract showed an antiproliferative effect on DLD-1 colorectal cancer cells. The suppression of cancer cell proliferation, in addition to enzyme inhibition, may be related to the simultaneous targeting of multiple biochemical pathways by polyphenolic compounds. While our preliminary study offers insights into the selective mechanism of action of the extract, it also identifies a need for further research. Specifically, it is essential to consider the effect of the extract on healthy cells and its potential therapeutic benefits[73]. In this regard, the selective predilection of cancer cells will be the focus of subsequent studies. All these findings indicate that *C. draba* extract can be used as a potential supplement in disorders such as diabetes, metabolic syndrome and hyperpigmentation and emphasise the need for further research that can form the basis for in vivo studies.

Conclusion

This study evaluated the potential of *Cardaria draba* (L.) DESV. subsp. *Chalepensis* (L.) extract to suppress both α-glucosidase and TRP1 using in vitro and in silico methods. Under controlled laboratory conditions, the results obtained with different doses of the extract indicated not only a marked decrease in enzyme activities, but also a decrease in the proliferation of DLD-1 colorectal cancer cells. Subsequent molecular dynamics simulations and protein-ligand interaction analyses were conducted to investigate the potential mechanisms underlying these effects.

The findings show that *Cardaria draba* (L.) DESV. subsp. *Chalepensis* (L.) extract, which has lower IC_{50} values than acarbos and kojic acid, which are considered as standard drug molecules, gives effective results in in vitro and in silico findings and needs to be confirmed by in vivo studies. New findings supported by in vivo experiments may lead to further inferences about the actual physiological effect of *C. draba* extract, especially through preclinical evaluations such as formulation stability and toxicity studies. The potential effect of the extract, especially on the α-glucosidase enzyme, indicates its potential use in the treatment of type 2 diabetes, and TRP1 inhibition indicates its potential use in the fight against hyperpigmentation and related dermatological problems. Molecular interaction studies provide potential data that flavonoids and phenolic compounds in the extract may conformationally destabilise the enzyme structures, which may significantly inhibit the functioning of the enzyme. Furthermore, the antiproliferative effect observed in DLD-1 cell line suggests that the extract may target more than one biochemical pathway. However, selectivity and formulation are important limitations that need to be further studied. In conclusion, *Cardaria draba* (L.) DESV. subsp. *Chalepensis* (L.) extract may be a candidate that may show potential for further in vivo studies in various therapeutic areas, including diabetes and skin diseases.

Data availability

The datasets generated and/or analysed during the current study are not publicly available due due to the limited reusability of the samples but are available from the corresponding author on reasonable request.

Received: 23 December 2024; Accepted: 21 March 2025
Published online: 26 March 2025

References

1. Jansson, P. A. Endothelial dysfunction in insulin resistance and type 2 diabetes. *J. Intern. Med.* **262** (2), 173–183. https://doi.org/10.1111/j.1365-2796.2007.01830.x (2007).
2. Vaish, U. et al. Micro RNAs upregulated in vitiligo skin play an important role in its aetiopathogenesis by altering TRP1 expression and Keratinocyte-Melanocytes cross-talk. *Sci. Rep.* **9** (1), 10079. https://doi.org/10.1038/s41598-019-46529-6 (2019).
3. Costa, R. et al. Xanthohumol modulates inflammation, oxidative stress, and angiogenesis in type 1 diabetic rat skin wound healing. *J. Nat. Prod.* **76** (11), 2047–2053. https://doi.org/10.1021/np4002898 (2013).
4. Zhou, Y. et al. Selaginellin inhibits melanogenesis via the MAPK signaling pathway. *J. Nat. Prod.* **85** (4), 838–845. https://doi.org/10.1021/acs.jnatprod.1c00971 (2022).
5. Liu, J., Pan, S., Wang, X., Liu, Z. & Zhang, Y. Role of advanced glycation end products in diabetic vascular injury: Molecular mechanisms and therapeutic perspectives. *Eur. J. Med. Res.* **28** (1), 553. https://doi.org/10.1186/s40001-023-01431-w (2023).
6. Su, J., Luo, Y., Hu, S., Tang, L. & Ouyang, S. Advances in research on type 2 diabetes mellitus targets and therapeutic agents. *Int. J. Mol. Sci.* **24** (17), 13381. https://doi.org/10.3390/ijms241713381 (2023).
7. Atanasov, A. G., Zotchev, S. B., Dirsch, V. M. & Supuran, C. T. Natural products in drug discovery: Advances and opportunities. *Nat. Rev. Drug Discov.*. **20** (3), 200–216. https://doi.org/10.1038/s41573-020-00114-z (2021).
8. Scurfield, G. Cardaria Draba (L.) Desv. *J. Ecol.* **50** (2), 489–499. https://doi.org/10.2307/2257459 (1962).
9. MULLIGAN, G. A. & FINDLAY, J. N. The biology of Canadian weeds. 3. Cardaria Draba, C. Chalepensis, and C. *Pubescens Can. J. Plant. Sci.* **54** (1), 149–160. https://doi.org/10.4141/cjps74-024 (1974).
10. Al-Shehbaz, I., Mutlu, B. & Dönmez, A. The Brassicaceae (Cruciferae) of Turkey, Updated. *Turk. J. Bot.* **31**(4), 327–336 (2007).

11. Aksakal, O., Sunar, S., Kaya, Y. & Agar, G. Genetic diversity within and among lepidium Draba populations from Eastern Anatolia based on RAPD analysis. *Biochem. Genet.* **48** (7–8), 603–611. https://doi.org/10.1007/s10528-010-9342-3 (2010).
12. Radonić, A. et al. Phytochemical analysis and antimicrobial activity of cardaria Draba (L.) Desv. *Volatiles Chem. Biodivers.* **8** (6), 1170–1181. https://doi.org/10.1002/cbdv.201000370 (2011).
13. Eruygur, N., Ayaz, F., Bağci, Y., Güler, E. & Maltaş Çağil, E. Phenolic composition, in-vitro antioxidant and enzyme Inhibition activities of cardaria Draba different parts. *Eur. J. Sci. Technol.* https://doi.org/10.31590/ejosat.1062109 (2022).
14. Nagata, C. et al. Skin pigmentation is inversely associated with insulin resistance in healthy Japanese women. *Diabetes Metab.* **42** (5), 368–371. https://doi.org/10.1016/j.diabet.2016.04.001 (2016).
15. Lehraiki, A. et al. Inhibition of melanogenesis by the antidiabetic Metformin. *J. Invest. Dermatol.* **134** (10), 2589–2597. https://doi.org/10.1038/jid.2014.202 (2014).
16. Ziegler, A. G. et al. Low-Pigment skin type and predisposition for development of type I diabetes. *Diabetes Care*. **13** (5), 529–531. https://doi.org/10.2337/diacare.13.5.529 (1990).
17. Kim, H. M. & Hyun, C. G. Drug repurposing of Voglibose, a diabetes medication for skin health. *Pharmaceuticals* **18** (2), 224. https://doi.org/10.3390/ph18020224 (2025).
18. Kumar, S., Narwal, S., Kumar, V. & Prakash, O. α-Glucosidase inhibitors from plants: A natural approach to treat diabetes. *Pharmacogn Rev.* **5** (9), 19–29. https://doi.org/10.4103/0973-7847.79096 (2011).
19. Laksmiani, N. P. L. & Nugraha, I. P. W. Depigmentation activity of Secang (Caesalpinia Sappan L.) extract through tyrosinase, tyrosinase related Protein–1 and dopachrome tautomerase Inhibition. *Biomedical Pharmacol. J.* **12** (2), 799–808 (2019).
20. Jin, T. Why diabetes patients are more prone to the development of colon. *Cancer? Med. Hypotheses*. **71** (2), 241–244. https://doi.org/10.1016/j.mehy.2008.03.025 (2008).
21. Shi, Y. & Hu, F. B. The global implications of diabetes and cancer. *Lancet* **383** (9933), 1947–1948. https://doi.org/10.1016/S0140-6736 (2014).
22. Yi, P. et al. Cyclopenta[Bc]Benzopyran derivatives and limonoids from Aglaia Edulis with cytotoxic and Anti-DENV activity. *J. Nat. Prod.* https://doi.org/10.1021/acs.jnatprod.4c01194 (2025).
23. Luque de Castro, M. D. & Priego-Capote, F. Soxhlet extraction: Past and present panacea. *J. Chromatogr. A*. **1217** (16), 2383–2389. https://doi.org/10.1016/j.chroma.2009.11.027 (2010).
24. Bakir Boga, O., Bugra Ortaakarsu, A., Kadırustaoglu, B. & Basaran Kurbanoglu, E. Phytochemical profiling, in vitro biological activities and in Silico molecular Docking studies of the crude extract of crambe orientalis, an endemic plant in Turkey. *Chem. Biodivers.* **20** (3), e202201142. https://doi.org/10.1002/cbdv.202201142 (2023).
25. Seraglio, S. K. T. et al. Development and validation of a LC-ESI-MS/MS method for the determination of phenolic compounds in honeydew honeys with the Diluted-and-Shoot approach. *Food Res. Int.* **87**, 60–67. https://doi.org/10.1016/j.foodres.2016.06.019 (2016).
26. Spanos, G. A. & Wrolstad, R. E. Influence of processing and storage on the phenolic composition of Thompson seedless grape juice. *J. Agric. Food Chem.* **38** (7), 1565–1571. https://doi.org/10.1021/jf00097a030 (1990).
27. Dewanto, V., Wu, X., Adom, K. K. & Liu, R. H. Thermal processing enhances the nutritional value of tomatoes by increasing total antioxidant activity. *J. Agric. Food Chem.* **50** (10), 3010–3014. https://doi.org/10.1021/jf0115589 (2002).
28. Chang, T. S., Ding, H. Y., Tai, S. S. K. & Wu, C. Y. Mushroom tyrosinase inhibitory effects of isoflavones isolated from soygerm Koji fermented with Aspergillus oryzae BCRC 32288. *Food Chem.* **105** (4), 1430–1438. https://doi.org/10.1016/j.foodchem.2007.05.019 (2007).
29. Daou, M. et al. Vitro α-Glucosidase inhibitory activity of tamarix Nilotica shoot extracts and fractions. *PLoS ONE*. **17** (3), e0264969. https://doi.org/10.1371/journal.pone.0264969 (2022).
30. Zengin, G. et al. Flavonoids, condensed tannins content of eight Centaurea species and their broad inhibitory activities against cholinesterase, tyrosinase, α-Amylase and α-Glucosidase. *Notulae Botanicae Horti Agrobotanici Cluj-Napoca*. **44** (1), 195–200. https://doi.org/10.15835/nbha44110259 (2016).
31. Mosmann, T. Rapid colorimetric assay for cellular growth and survival: Application to proliferation and cytotoxicity assays. *J. Immunol. Methods*. **65** (1), 55–63. https://doi.org/10.1016/0022-1759 (1983).
32. Ortaakarsu, A. B. & MedetalıBeyoğlu, H. Computational drug repurposing effort for identifying novel hits for the treatment of diseases such as endometriosis, uterine fibroids, and prostate cancer. *Turk. J. Chem.* **48** (2), 402–421. https://doi.org/10.55730/1300-0527.3659 (2024).
33. Kızıltaş, H. et al. Sage (Salvia Macrochlamys): LC-HRMS for phytochemical analysis, cytotoxicity, enzyme inhibition, antioxidant activity, molecular docking and molecular dynamics simulations. *Plant. Biosyst. nt. J. Dealing all Aspects Plant. Biol.* https://doi.org/10.1080/11263504.2024.2386337
34. Kiziltaş, H. et al. Chemical profiling by LC-HRMS, antioxidant potential, enzyme Inhibition, molecular Docking and molecular dynamics simulations of Acantholimon Acerosum. *J. Mol. Struct.* 140124. https://doi.org/10.1016/j.molstruc.2024.140124 (2024).
35. Sel, S. et al. Acetohydroxyacid synthase (AHAS) inhibitor-based commercial sulfonylurea herbicides as glutathione reductase inhibitors: In vitro and in silico studies. *ChemistrySelect* **7** (38), e202202235 https://doi.org/10.1002/slct.202202235 (2022).
36. Yagiz, G. et al. Inhibition properties against Xanthine oxidase and molecular Docking studies of dimethyl N-Benzyl–1H–1,2,3-Triazole–4,5-Dicarboxylate and (N-Benzyl–1H–1,2,3-Triazole–4,5-Diyl)Dimethanol derivatives. *Bioorg. Chem.* **108**, 104654. https://doi.org/10.1016/j.bioorg.2021.104654 (2021).
37. Kalin, T. N. et al. Molecular modeling studies, ADME prediction of arachidonic acid carbamate derivatives, and evaluation of their acetylcholinesterase activity. *Drug Dev. Res.* **81** (2), 232–241. https://doi.org/10.1002/ddr.21621 (2020).
38. Schrödinger Release 2023–4: Maestro, (Schrödinger, LLC, New York, NY, 2023).
39. Schrödinger Release 2023–4: LigPrep, (Schrödinger, LLC, New York, NY, 2023).
40. Schrödinger Release 2023–4: Epik, *Schrödinger, LLC, New York, NY, 2023).
41. Lu, C. et al. OPLS4: Improving force field accuracy on challenging regimes of chemical space. *J. Chem. Theory Comput.* **17** (7), 4291–4300. https://doi.org/10.1021/acs.jctc.1c00302 (2021).
42. Lai, X., Wichers, H. J., Soler-Lopez, M. & Dijkstra, B. W. Structure of human tyrosinase related protein 1 reveals a binuclear zinc active site important for melanogenesis. *Angew. Chem. Int. Ed.* **56** (33), 9812–9815. https://doi.org/10.1002/anie.201704616 (2017).
43. Karade, S. S. et al. N-Substituted valiolamine derivatives as potent inhibitors of Endoplasmic reticulum α-Glucosidases I and II with antiviral activity. *J. Med. Chem.* **64** (24), 18010–18024. https://doi.org/10.1021/acs.jmedchem.1c01377 (2021).
44. Zamanos, A., Ioannakis, G. & Emiris, I. Z. HydraProt: A new deep learning tool for fast and accurate prediction of water molecule positions for protein structures. *J. Chem. Inf. Model.* **64** (7), 2594–2611. https://doi.org/10.1021/acs.jcim.3c01559 (2024).
45. Schrödinger, R. et al. Protein Preparation Wizard, 2023, LLC, New York, NY; (Schrödinger, LLC, New York, NY, 2023).
46. Schrödinger Release 2023–4: Induced Fit Docking Protocol; Glide, (Schrödinger, LLC, New York, NY & Prime Schrödinger, LLC, New York, NY, 2023).
47. Mark, P. & Nilsson, L. Structure and dynamics of the TIP3P, SPC, and SPC/E water models at 298 K. *J. Phys. Chem. A*. **105** (43), 9954–9960. https://doi.org/10.1021/jp003020w (2001).
48. The Nose–Hoover thermostat | The Journal of Chemical Physics | AIP Publishing. https://pubs.aip.org/aip/jcp/article-abstract/83/8/4069/219065/The-Nose-Hoover-thermostatThe-Nose-Hoover?redirectedFrom=fulltext (Accessed 01 Jan 2024).
49. Martyna, G. J., Tobias, D. J. & Klein, M. L. Constant pressure molecular dynamics algorithms. *J. Chem. Phys.* **101** (5), 4177–4189. https://doi.org/10.1063/1.467468 (1994).

50. Schrödinger, R. & Shaw, D. E. *Research 2023–4: Desmond Molecular Dynamics System, New York, NY, Maestro-Desmond Interoperability Tools*, (Schrödinger, 2023).
51. Medetalibeyoğlu, H. et al. Design, and cholinesterase inhibitory activity of novel 1,2,4-Triazole schiff bases: A combined experimental and computational approach. *Int. J. Biol. Macromol.* **306**, 141350. https://doi.org/10.1016/j.ijbiomac.2025.141350 (2025).
52. Coifman, R. R., Kevrekidis, I. G., Lafon, S., Maggioni, M. & Nadler, B. Diffusion maps, reduction coordinates, and low dimensional representation of stochastic systems. *Multiscale Model. Simul.* **7** (2), 842–864. https://doi.org/10.1137/070696325 (2008).
53. Schultze, S. & Grubmüller, H. Time-Lagged independent component analysis of random walks and protein dynamics. *J. Chem. Theory Comput.* **17** (9), 5766–5776. https://doi.org/10.1021/acs.jctc.1c00273 (2021).
54. Li, J. et al. The VSGB 2.0 model: A next generation energy model for high resolution protein structure modeling. *Proteins Struct. Funct. Bioinform.* **79** (10), 2794–2812. https://doi.org/10.1002/prot.23106 (2011).
55. Schrödinger Release 2023–4: Prime, Schrödinger, LLC, New York, NY, (2023).
56. Johnston, B. et al. C. R.; zachcp. BradyAJohnston/MolecularNodes: V4.2.12 for Blender 4.2+, (2025). https://doi.org/10.5281/zenodo.14873613
57. Michaud-Agrawal, N., Denning, E. J., Woolf, T. B. & Beckstein, O. MDAnalysis: A toolkit for the analysis of molecular dynamics simulations. *J. Comput. Chem.* **32** (10), 2319–2327. https://doi.org/10.1002/jcc.21787 (2011).
58. Yue, Z. et al. Comparative study of the quality indices, antioxidant substances, and mineral elements in different forms of cabbage. *BMC Plant. Biol.* **24** (1), 187. https://doi.org/10.1186/s12870-024-04857-4 (2024).
59. Gunjal, M. et al. Assessment of bioactive compounds, antioxidant properties and morphological parameters in selected microgreens cultivated in soilless media. *Sci. Rep.* **14** (1), 23605 (2024).
60. Khan, P. & Akhtar, N. Phytochemical investigations and development of ethosomal gel with brassica oleraceae L.(Brassicaceae) extract: An innovative nano approach towards cosmetic and pharmaceutical industry. *Ind. Crops Prod.* **183**, 114905 (2022).
61. Arena, P. et al. Comparative study on phenolic profile and biological activities of the aerial parts of sinapis pubescens L. Subsp. pubescens (Brassicaceae) wild from Sicily (Italy). *Chem. Biodivers.* **20** (6), e202300309. https://doi.org/10.1002/cbdv.202300309 (2023).
62. Eroglu, P., Alzaim, M. & Binzet, R. Total phenolic content, phytochemical profile and cytotoxic effects of endemic alyssum floribundum (Brassicaceae) from Turkey. *Plant. Biosyst. Int. J. Dealing Aspects Plant. Biol.*. **158** (4), 641–649. https://doi.org/10.1080/11263504.2024.2347855 (2024).
63. Narvaez, J. J. U. et al. Identification of bioactive compounds in Brassica Oleracea Var. Capitata L. with enzyme-inhibitory activity against postprandial hyperglycemia. *Fitoterapia* 106343. (2024).
64. Okumus, E. Effect of ultrasonic and conventional extraction on bioactive components, glucosinolate content and antidiabetic activity of crambe Tataria. *Fitoterapia* **178**, 106177 (2024).
65. Placines, C. et al. Phenolic profile, toxicity, enzyme Inhibition, in Silico studies, and antioxidant properties of cakile maritima Scop. (Brassicaceae) from Southern Portugal. *Plants* **9** (2), 142 (2020).
66. Meriç, Z., Özdemir Nath, E., Doğan, A. & Bitiş, L. Antioxidant Anti-Tyrosinase activities and characterization of phenolic compounds for some plants from the Marmara region, Türkiye. *J. Res. Pharm.* **28** (2), 396-408 (2024).
67. KOYU, H. Supercritical carbon dioxide extraction optimization of brassica Oleracea Var. Capitata F. Rubra leaf extracts F.r cholinesterase and tyrosinase inhibitory activity. *J. Res. Pharm.* **28** (2), 458-469 (2024).
68. Lai, X., Wichers, H. J., Soler-Lopez, M. & Dijkstra, B. W. Structure and function of human tyrosinase and tyrosinase-Related proteins. *Chem. Eur. J.* **24** (1), 47–55. https://doi.org/10.1002/chem.201704410 (2018).
69. Nazeam, J. A. & EL-Emam, S. Z. Middle Eastern plants with potent cytotoxic effect against lung cancer cells. *J. Med. Food.* **27** (2), 198–207. https://doi.org/10.1089/jmf.2022.0098 (2024).
70. Abdulaziz, N. T., Mohammed, E. T., Khalil, R. R. & Mustafa, Y. F. Unrevealing the total phenols, total flavonoids, antioxidant, Anti-Inflammatory, and cytotoxic effects of garden Cress seed ethanolic extracts. *Rev. Clin. Pharmacol. Pharmacokinet. Int. Ed.* **38** (2), 187–196 (2024).
71. Oraby, E. & Radwan, O. P. Constituents and cytotoxic effects of brassica juncea extract on different human cancer cell lines in vitro. *Biol. Biomed. J.* **2** (2), 148–155 (2024).
72. Ravishankar, D., Rajora, A. K., Greco, F. & Osborn, H. M. I. Flavonoids as prospective compounds for Anti-Cancer therapy. *Int. J. Biochem. Cell Biol.* **45** (12), 2821–2831. https://doi.org/10.1016/j.biocel.2013.10.004 (2013).
73. Dilkalal, A., Annapurna, A. S. & Umesh, T. G. In vitro antioxidant, anticancer and in Silico studies of polyphenol enriched leaf extract of asystasia gangetica. *Sci. Rep.* **14** (1), 28374. https://doi.org/10.1038/s41598-024-79996-7 (2024).

Author contributions

Responsibilities and Contributions: Each author has significantly contributed to the research, analysis, and writing of this manuscript. The specific contributions of each author are as follows:. A. B. O.: Formal Analysis, Review and Writing, Validation, Computable Analysis, in silico Studies, Interpretation of Experimental Data, Verification. Ö. B. B.: Experiments, methodology, interpretation of experimental results. E. B. K.: Review, Project Management.

Declarations

Competing interests

The authors declare no competing interests.

Generative AI and AI-assisted technologies in the writing proces

During the preparation of this work, the author(s) used DeepL Pro and DeepL Write to enhance the academic tone and readability of the manuscript in English. After using these tools, the author(s) reviewed and edited the content as needed and take(s) full responsibility for the content of the published article.

Additional information

Supplementary Information The online version contains supplementary material available at https://doi.org/10.1038/s41598-025-95538-1.

Correspondence and requests for materials should be addressed to A.B.O.